Research Square

Preprints are preliminary reports that have not undergone peer review.
They should not be considered conclusive, used to inform clinical practice,
or referenced by the media as validated information.

# MALAT1 is required for estradiol to act as a mitogen in hormone receptor-positive breast cancer

**Sara De Martino**
National Research Council
**Aurora Aiello**
National Research Council
**Veronica Barbi**
Università Cattolica del Sacro Cuore
**Luca Cis**
National Research Council
**Valeria Pecci**
Università Cattolica del Sacro Cuore
**Antonio Franco**
Agostino Gemelli University Polyclinic
**Marcello Pompa**
National Research Council
**Melissa Borsa**
Università Cattolica del Sacro Cuore
**Roberta Benvenuto**
Agostino Gemelli University Polyclinic
**Angela Santoro**
Agostino Gemelli University Polyclinic
**Gianluca Franceschini**
Agostino Gemelli University Polyclinic
**Andrea De Gaetano**
National Research Council
**Simona Panunzi**
National Research Council
**Alessandra Fabi**
Agostino Gemelli University Polyclinic
**Sandra Atlante**
Istituti Clinici Scientifici Maugeri
**Carlo Gaetano**

Istituti Clinici Scientifici Maugeri

**Simona Nanni**

Università Cattolica del Sacro Cuore

**Antonella Farsetti**

antonella.farsetti@cnr.it

National Research Council

---

**Article**

**Keywords:** MALAT1, lncRNA, hormone receptor-positive breast cancer, 17β-estradiol, estrogen-driven proliferation, androgen receptor, estrogen receptor alpha, RNA immunoprecipitation, receptor-containing ribonucleoprotein complexes, receptor redistribution, ME3, PTGS2/COX-2, primary breast cancer cultures, nonlinear mixed-effects growth models

**Posted Date:** October 23rd, 2026

**DOI:** https://doi.org/10.21203/rs.3.rs-11243326/v1

**License:** This work is licensed under a Creative Commons Attribution 4.0 International License. Read Full License

**Additional Declarations:** No competing interests reported.

---

# MALAT1 is required for estradiol to act as a mitogen in hormone receptor-positive breast cancer

Sara De Martino[1], Aurora Aiello[1], Veronica Barbi[2,3], Luca Cis[1], Valeria Pecci[2], Antonio Franco[4], Marcello Pompa[1], Melissa Borsa[2], Roberta Benvenuto[4], Angela Santoro[4], Gianluca Franceschini[4], Andrea De Gaetano[1,5], Simona Panunzi[1], Alessandra Fabi[4], Sandra Atlante[1,3], Carlo Gaetano[3,6], Simona Nanni[2,4*] and Antonella Farsetti[1]*

[1] Consiglio Nazionale delle Ricerche, Istituto di Analisi dei Sistemi e Informatica, "A. Ruberti", (CNR)-IASI, Rome, Italy; [2]Department of Translational Medicine and Surgery, Università Cattolica del Sacro Cuore, Rome, Italy; [3]Laboratory of Epigenetics, Istituti Clinici Scientifici Maugeri IRCCS, Pavia, Italy, [4]Fondazione Policlinico Gemelli IRCCS, Rome, Italy, [5] North-West University, Focus Area for Pure and Applied Analytics, Potchefstroom, South Africa; [6] Departmental Faculty of Medicine, Saint Camillus International University of Health and Medical Sciences, Rome, Italy.

* AF and SN co-corresponding authors

**Address correspondence to:** Antonella Farsetti, CNR-IASI c/o Università Cattolica del Sacro Cuore, Largo F. Vito 1, 00168 Rome, Italy, Phone: +39 0630159964, Mail: antonella.farsetti@cnr.it and Simona Nanni, Department of Translational Medicine and Surgery, Università Cattolica del Sacro Cuore, Largo F. Vito 1, 00168 Rome, Italy; Phone: +39 0630154165, Mail: simona.nanni@unicatt.it.

**Keywords:** MALAT1; lncRNA; hormone receptor-positive breast cancer; 17β-estradiol; estrogen-driven proliferation; androgen receptor; estrogen receptor alpha; RNA immunoprecipitation; receptor-containing ribonucleoprotein complexes; receptor redistribution; ME3; PTGS2/COX-2; primary breast cancer cultures; nonlinear mixed-effects growth models.

**Abstract**

Breast cancer (BC) is the most common female malignancy with ~70% of cases hormone-receptor positive (HR+). We identify long noncoding RNA MALAT1 as a modulator of estrogen-driven proliferation in HR+ BC. We analyzed longitudinal IncuCyte data using cell-line-specific nonlinear mixed-effects growth models. MALAT1 targeting alone significantly reduced proliferation in MCF7 cells, whereas it had no significant basal effect in T47D, LNCaP, or 22RV1 cells. 17β-estradiol (E2) stimulated proliferation in LacZ gapmer controls in both MCF7 and T47D cells, but this mitogenic response was significantly reduced after MALAT1 depletion. Across five patient-derived Luminal B breast cancer cultures, MALAT1-targeted cells remained growth-suppressed despite E2 exposure and frequently displayed increased Annexin V signal. Mechanistically, MALAT1 depletion reduced ME3 and increased PTGS2/COX-2, with maximal PTGS2/COX-2 mRNA and enzymatic activity induction when combining MALAT1 targeting + E2 in MCF7. Increased IL-6 and CASP8 was consistent with a stress-associated inflammatory and cell-death response. Chromatin immunoprecipitation revealed cell-line- and locus-specific remodeling of ERα and AR occupancy; enzalutamide partially attenuated PTGS2 induction in MALAT1-targeted + E2, whereas PTGS2 knockdown increased cell-death susceptibility in selected conditions. These findings identify MALAT1 as a permissive regulator of estrogen-driven proliferation and nominate the MALAT1-ME3-COX-2 axis as a candidate vulnerability in HR+ BC.

## 1. Introduction

Breast cancer affects approximately 2.3 million women annually and accounts for around 670,000 deaths globally [1]. Its molecular heterogeneity underpins distinct clinical behaviors: HR+ tumors expressing estrogen receptor alpha (ERα) and/or progesterone receptor (PR) constitute the most common subtype (~70%) and are primarily managed with endocrine therapies, including selective estrogen receptor modulators (SERMs) such as tamoxifen, aromatase inhibitors, and selective ER degraders [2]. Although these approaches yield durable responses in many patients, intrinsic and acquired resistance remain major unresolved clinical challenges, driving the search for complementary molecular targets.

Long non-coding RNAs (lncRNAs) are recognized as key regulators of chromatin structure, transcriptional programs, and post-transcriptional gene regulation [3]. Among them, Metastasis-Associated Lung Adenocarcinoma Transcript 1 (MALAT1), a highly conserved and abundantly expressed nuclear lncRNA located on chromosome 11q13, has been linked to tumor progression, metastasis, and therapy resistance [4,5]. In breast cancer, MALAT1 has a context-dependent role: most studies describe oncogenic functions that promote proliferation, invasion, and treatment resistance [6–8], whereas genetic knockout in transgenic models has also revealed metastasis-suppressive activity through transcriptional enhanced associate domain (TEAD) inactivation [9]. In triple-negative breast cancer (TNBC), single-cell profiling associated multiple MALAT1 transcripts with persistence during neoadjuvant chemotherapy, while MALAT1 promoter deletion increased sensitivity to paclitaxel and doxorubicin and broadly remodeled metabolic and angiogenic programs [10]. These findings support the idea that MALAT1's biological consequences depend on cellular subtype, hormonal context, and treatment pressure.

Our group previously identified MALAT1 as a key metabolic regulator in prostate cancer (PCa). Its depletion reduces several metabolic enzymes, including choline kinase alpha (CHKA), ceramide kinase (CERK), pyruvate dehydrogenase kinases, and, most notably, malic enzyme 3 (ME3), thereby inhibiting PCa-cell proliferation [11,12]. Although prostate and breast cancers are primarily driven by androgen and estrogen signaling, respectively, both tumor types can endogenously express ERα and AR [13,14]. We therefore hypothesized that MALAT1-dependent metabolic and receptor-regulatory networks might also operate in HR+ breast cancer, while retaining important cell-type-specific features.

Prostaglandin-endoperoxide synthase 2 (*PTGS2*), which encodes the inducible enzyme cyclooxygenase COX-2, is a crucial inflammatory enzyme that catalyzes the production of prostaglandin H2 (PGH2) from arachidonic acid, and functions as both a dioxygenase and a peroxidase [15]. COX-2 is overexpressed in many human cancers - including breast cancer - where it supports cell survival, growth, and anti-apoptotic signaling primarily through its downstream effector prostaglandin E2 (PGE2) [16–19]. Notably, ERα signaling has been shown to transcriptionally upregulate *PTGS2* in mammary cells [20,21], linking the estrogen pathway directly to prostaglandin-driven cancer development. The role of MALAT1 in this regulatory circuit remains unexplored.

ME3 is a mitochondrial NADP+-dependent malic enzyme that converts malate to pyruvate and produces NADPH, a vital reducing agent for mitochondrial antioxidant defense [22]. Cancer cells rely on NADPH for glutathione recycling and ROS detoxification, making ME family members attractive metabolic targets [23]. Loss of mitochondrial NADPH, caused by ME2 or ME3 knockdown, increases intracellular ROS and triggers apoptosis in various cancer models [24,25].

In this study, we asked whether MALAT1 is required for HR+ breast cancer cells to translate estrogen-receptor activation into a proliferative response. We compared the effects of MALAT1 targeting under basal and hormone-stimulated conditions and examined associated changes in ME3 and PTGS2/COX-2 expression, COX-2 activity, inflammatory-stress markers, and ERα/AR promoter occupancy. To assess the relevance of the findings beyond established cell lines, we also analyzed immunophenotypically characterized primary epithelial cultures derived from fresh biopsies of five patients with heterogeneous Luminal B tumors. Finally, PTGS2/COX-2 co-targeting was used to test whether COX-2 contributes to survival after MALAT1 depletion. This integrated approach was designed to distinguish a general antiproliferative effect of MALAT1 loss from a specific requirement for MALAT1 in estrogen-driven growth.

## Materials and Methods

### Cell Lines and Culture Conditions

We cultured T47D and MCF7 cells in DMEM and MEM, respectively. LNCaP and 22Rv1 cells were cultured in RPMI-1640 medium (Corning, New York, NY, USA; Cat. No. 10-040-CV). All media were supplemented with 10% fetal bovine serum (FBS; Gibco, Invitrogen, Carlsbad, CA, USA; Cat. No. 10270106), 1% L-glutamine (Corning; Cat. No. 25-005-CI), and 1% penicillin-streptomycin (Corning; Cat. No. 30-002-CI). In addition, LNCaP and 22Rv1 media were supplemented with 1% HEPES (Corning; Cat. No. 25-060-CI), while 22Rv1 medium was further supplemented with 1% sodium pyruvate (Corning; Cat. No. 25-000-CIR) and 1% glucose. We acquired cell lines from the American Type Culture Collection (ATCC). Cells were incubated at 37°C with 5% $CO_2$. We routinely used indirect (Hoechst) methods to screen all cell lines for mycoplasma contamination. At least 72 h before use, cells were switched to a medium with hormone-deprived serum (SS) as in [12,26] and treated with 5α-dihydrotestosterone (DHT) (NMID, Sydney, NSW, AU, #680), 17β-estradiol (E2) and enzalutamide (ENZ) at the concentrations and times indicated in the figure legends, or vehicle (ethanol) as a negative control. We silenced MALAT1 using specific LNA gapmers, as previously described in [26]. We used LacZ gapmers as a non-targeting control [11].

### Primary cultures and immunocytochemistry

Primary epithelial cultures were established from breast cancer biopsy specimens obtained from patients undergoing neoadjuvant therapy at Fondazione Policlinico Gemelli (FPG) -IRCCS, Rome, Italy. All tumors were classified as Luminal B; **Table 1** reports the clinical and pathological characteristics of the patients and tumors.

The Lazio Area 3 Territorial Ethics Committee of Rome, Italy has authorized patient's enrollment and the establishment of primary cultures - (Protocol number: ID 6269; N.0000006/24, approved January 5, 2024) and written informed consent was obtained from each patient in the presence of a physician providing explanation. All procedures were conducted according to the principles expressed in the Declaration of Helsinki, institutional regulation, and Italian laws and guidelines.

We established cultures using the EpiCult™-C Human Medium Kit (STEMCELL Technologies) according to the manufacturer's protocol. We characterized the cultures by Western blotting and immunocytochemistry; their immunophenotypic profiles are summarized in **Table 2**.

**Table 1. Clinical and pathological characteristics of the patients and tumors from which the primary cultures were established.**

| Primary culture | Age | Histotype | Subtype | ERα % (biopsy*) | PR % (biopsy*) | AR % (biopsy*) | Ki67 % (biopsy*) |
|---|---|---|---|---|---|---|---|
| EPG5 | 48 | Invasive lobular | Luminal B | 85 | 85 | 30 | 30 |
| EPG9 | 54 | Invasive ductal | Luminal B | 90 | <1 | 45 | 50 |
| EPG11 | 43 | Invasive ductal | Luminal B | 85 | 80 | 30 | 45 |
| EPG25 | 65 | Invasive ductal | Luminal B | 95 | 85 | 95 | 40 |
| EPG43 | 59 | Invasive ductal | Luminal B | 40 | 55 | 90 | 22 |
| EPG55 | 39 | Invasive ductal | Luminal B | 90 | 90 | 90 | 65 |

Abbreviations: ERα, estrogen receptor alpha; PR, progesterone receptor; AR, androgen receptor. *Biopsy values indicate the percentage of positive cells in the original tumor-tissue biopsy.

**Table 2. Immunophenotypic characterization of Luminal B primary epithelial cultures by Western blotting and immunocytochemistry.**

| Primary culture | ERα (WB*) | AR (WB*) | E-cad (WB*) | Vimentin (WB*) | α-SMA (WB*) | CK8/18 (ICC#) | CK19 (ICC#) | CK14 (ICC#) |
|---|---|---|---|---|---|---|---|---|
| EPG5 | ++ | + | + | + | – | Isolated elements | Positive | Few positive cells |
| EPG9 | ++ | + | + | ++ | – | Isolated elements | Isolated elements | Isolated elements |
| EPG11 | ++ | + | +++ | – | – | Negative | Isolated elements | Isolated elements |
| EPG25 | ++ | + | + | + | – | Negative | ND | ND |
| EPG43 | ++ | + | + | + | – | Negative | ND | ND |
| EPG55 | ++ | + | ++ | + | – | Negative | Isolated elements | Focal/isolated elements |

Abbreviations: WB, Western blotting; ICC, immunocytochemistry; E-cad, E-cadherin; α-SMA, alpha-smooth-muscle actin; CK, cytokeratin; ND, not determined. *WB scoring: −, negative; +, weak; ++, moderate; +++, strong expression. #ICC scoring describes the distribution of positive cells.

Immunocytochemical staining was performed on the Ventana automated immunostainer (Ventana BenchmarK Ultra, Tucson, AZ, USA) and the Leica Bond III. The following antibodies were applied for 60 min: Anti-Estrogen receptor, clone SP1, Ventana Roche RTU; Anti-Androgen Receptor, clone SP107, Ventana Roche RTU; Anti-Cytokeratin 14, clone SP53, Ventana Roche

RTU; Anti-Cytokeratin 19, clone A53-B/A2, Ventana Roche RTU; Anti-Cytokeratin 8/18, clone 5D3, Leica RTU. Diaminobenzidine was used as the chromogen, and sections were counterstained with hematoxylin. We included positive controls in each immunostaining run.

### *PTGS2*/COX-2 Functional Inhibition and Enzymatic Activity

Genetic knockdown of *PTGS2*/COX-2 was achieved by co-transfecting a *PTGS2*-targeting siRNA or the NC1 control using the TriFECTa RNAi Kit (Integrated DNA Technologies) together with MALAT1 or LacZ gapmers in hormone-deprived MCF7 and T47D cells. Cells were quantified manually using a trypan blue exclusion test of cell viability (Gibco #15250061) at the experimental endpoint under vehicle, E2, or DHT conditions.

COX-2 enzymatic activity was assessed using the fluorometric assay ab204699 (Abcam), which measures the conversion of arachidonic acid to PGH2. MCF7 and T47D cells treated with LacZ or MALAT1 gapmer, with or without E2 (10 nM), were harvested in ice-cold PBS, counted, and lysed in 1% IGEPAL CA-630 in PBS containing protease inhibitors. Lysates were clarified at 12,000×g for 3 min and transferred in duplicate to 96-well plates. Parallel reactions were performed in the presence or absence of celecoxib as COX-2-specific assay control. Arachidonic acid was added to initiate the reaction, and fluorescence was recorded (Ex/Em 535/587 nm) every 15 min for 3 h using a GloMax Discover Microplate Reader (Promega). We normalized fluorescence values to the number of cells used for each condition.

### Proliferation Assays

We assessed proliferation using the IncuCyte S3 Live-Cell Analysis System (Sartorius, Essen BioScience, Ann Arbor, MI, USA). Briefly, cells were seeded in triplicate in 48-well plates (Corning, Cat. No. 3548), and images were acquired every 2 or 6 h for up to 7 days. We analyzed images using the IncuCyte Cell-by-Cell Analysis Software (version 2022b Rev2).

For apoptosis analysis, we added IncuCyte Annexin V NIR Dye (Cat. No. 4768) according to the manufacturer's instructions on day 3 and acquired images every 6 hours for up to 4 days. Apoptotic cells were identified and quantified based on Annexin V NIR fluorescence intensity acquired by the IncuCyte Live-Cell Analysis System. The software's integrated analysis algorithm calculated the apoptotic index.

**Gene Expression Analysis**

Total RNA was extracted using TRIzol Reagent (Thermo Fisher Scientific, Waltham, MA, USA) according to the manufacturer's instructions. cDNA was generated with the High-Capacity cDNA Reverse Transcription Kit (Applied Biosystems, Foster City, CA, USA), and qRT-PCR was performed using SYBR Green on a QuantStudio 5 (QS5) or QuantStudio 7 (QS7) Pro Real-Time PCR System (Applied Biosystems). We performed amplification and melting-curve analyses as previously described [11]. Relative expression was calculated by the $2^{-\Delta Ct}$ method and is reported as fold change relative to LacZ vehicle unless otherwise indicated. Primers were as follows:

hFKBP5 5'-CCATTTGTCTTTAGTCTTGGCAAA-3' and 5'- ATGGTAGCCACCCCAATGTC-3';

hERα 5'-GGGAAGCTACTGTTTGCTCCTAAC-3'and 5'-CACCATGCCCTCTACACATTTTC-3';

hPTGS2 5'-GAATCATTCACCAGGCAAATTG-3'and 5'-TGCGGGTGGAACATTCCTA-3';

hME1 5'-CAATGCATGGCCAGAAGATGT-3'and 5'-CCAAGAATACGCTCTCCATCAGT-3';

hME2 5'-CCTCTCCGCCGGGTGTA-3'and 5'-ACCGGGACAACATCTTTTCTTTC-3'.

Primers for MALAT1, *PS2*, and *GAPDH*, *P0*, were as in [26]. *AR* as in [27], *ME3* as in [11].

**Protein Extraction and Western Blotting**

We prepared total protein lysates using standard detergent-based extraction procedures as in [12]. We separated 15 µg of protein by SDS-PAGE and transferred it for immunoblotting. Signals were developed using ECL Prime (Amersham, GE Healthcare) and acquired with an iBright Imaging System (Thermo Fisher Scientific). Densitometry was performed with ImageJ and normalized to the β-actin loading control

Antibodies: AR (1:1000, Merk Millipore, #06680); ERα [HC-20] (1:1000, Santa Cruz, #sc-543), ERα [D8H8] (1:1000, Cell Signaling, #8644), ME3 (1:1000, Abcam,#172972), COX2 [F1F3H] (1:1000, Cell signaling, #43542), COX2 [D5H5] (1:1000, Cell signaling, #12282), Vimentin [V9] (1:1000, Cell signaling, #49636), α-Smooth Muscle Actin [1A4] (1:1000, Cell signaling, #56856), .β-actin (1:8000, Sigma, #1305556), E-cadherin (1:1000, GeneTex, # GTX100443, and Abcam, [4A2], #231303), Goat anti-Mouse IgG HRP (Bio-Rad Cat# 170–6516,), and Goat-anti-Rabbit IgG HRP (SeraCare KPL, #5220 − 0336).

**Chromatin Immunoprecipitation (ChIP)**

MCF7 and T47D cells were cross-linked with 1% formaldehyde for 10 min at room temperature (RT), then quenched with glycine for 5 min at RT. Following PBS washes, cells were lysed (50 mM Hepes, pH 7.9, 140 mM NaCl, 1 mM EDTA, pH 8.0, 10% $^{v}/_{v}$ Glycerol, 0.5% $^{v}/_{v}$ NP-40, 0.25% $^{v}/_{v}$ Triton X-100, and protease inhibitors), and a pellet of nuclei was recovered by centrifugation. The nuclei were washed twice with 1 mL of ice-cold wash buffer (10 mM Tris-HCl, pH 8.0, 200 mM NaCl, 1 mM EDTA, pH 8.0, 0.5 mM EGTA, pH 8.0, and protease inhibitors) and resuspended in 300 µL of ice-cold shearing buffer (0.1% w/v SDS, 1 mM EDTA, 10 mM Tris-HCl, pH 8.0, and protease inhibitors). Chromatin was fragmented by sonication using a Bioruptor Pico (Diagenode) 30'' ON/30'' OFF for 15 cycles to obtain fragments of approximately 1000 bp, as verified by agarose gel electrophoresis.

After pre-clearing with Magna ChIP Protein A+G magnetic beads (Sigma-Aldrich, #16-663) for 1 hour at 4°C, chromatin was incubated overnight at 4°C with the indicated antibodies and captured with Protein A+G magnetic beads for 2 hours. Immunocomplexes were sequentially washed with low-salt, high-salt, LiCl, and TE buffers on a magnetic stand. Complexes were eluted in 10 mM Tris-HCl (pH 8.0), 0.3 M NaCl, 5 mM EDTA, and 0.5% SDS. Cross-links were reversed overnight at 65°C after addition of NaCl, followed by RNase (Invitrogen, #12091021**)** and proteinase K (Invitrogen, #25530049) treatment.

DNA fragments were recovered using phenol-chloroform and analyzed by quantitative qPCR on a QuantStudio 5 Real-Time PCR System (Applied Biosystems) using SYBR Master Mix (Applied Biosystems, Foster City, CA, USA) with the evaluation of dissociation curves [11,12]. Standard curves were generated by serially diluting the input (5-log dilutions in 2 triplicate), and data were represented as relative enrichment.

Immunoprecipitations were performed with antibodies against ERα D8H8 (Cell Signaling, #8644; 5 microgram/sample), AR (Abcam, #ab19066; 6 microgram/sample), and AR D6F11 (Cell Signaling, #5153; 6 microgram/sample). Rabbit IgG (Bethyl, #P120-101) or donkey anti-goat IgG (Abcam, #ab6885) served as negative controls. Primer sequences are listed below:

hME3 Prom 5'-AACACACACCTGGAGTCATCAAA-3'and 5'-TTGGCTGGGCTGTTCTCTCT-3';
hPTGS2 Prom 5'-GGAGGAGAGGGGAGGGATCAG-3'and 5'-AGGAAG CTG CCCCAATTTG-3';
Primer for the PS2 promoter, as in [26].

**Statistical Analysis**

We analyzed longitudinal IncuCyte proliferation data collected after treatment using nonlinear mixed-effects growth models [28]. Proliferation measurements were normalised to the pre-treatment baseline value for each experimental unit and condition. For LNCaP and T47D, the normalized response was expressed as a percentage of baseline, with the baseline value set to 100%; for MCF7 and 22RV1, these percentages were further shifted by 100 percentage points so that the baseline value was 0%, consistently with the zero-origin Hill growth function. An exponential growth model was used for the LNCaP and T47D cell lines, whereas a Hill growth model was used for the MCF7 and 22RV1 cell lines. For LNCaP and T47D, the exponential model included condition-specific fixed effects of the six gapmer–hormone conditions on the exponential growth-rate parameter $\boldsymbol{\lambda}$, whereas the initial response parameter $\boldsymbol{A}$ was estimated at the population level. Condition-dependent random effects for $\boldsymbol{\lambda}$ were included at the experimental-unit level to account for between-experiment variability in growth rates across experimental conditions. For MCF7, the Hill model included condition-specific fixed effects for the asymptotic response $\boldsymbol{K}$ and the half-response time $\boldsymbol{t_{50}}$, whereas the Hill coefficient $\boldsymbol{h}$ was assumed to be common across conditions and experimental units. Experiment-level random effects for $\mathbf{log}(\boldsymbol{t_{50}})$, including condition-dependent deviations within experimental units, were included to account for between-experiment variation in the temporal dynamics of growth. For 22RV1, for which only two experimental units were available, a reduced Hill model was fitted. This model retained condition-specific fixed effects for $\boldsymbol{K}$, whereas the population-average parameters $\boldsymbol{t_{50}}$ and $\boldsymbol{h}$ were assumed to be common across conditions. Experiment-level random effects for $\mathbf{log}(\boldsymbol{t_{50}})$, including condition-dependent deviations, were retained. All nonlinear parameters were estimated on the logarithmic scale and back-transformed within the corresponding model function to ensure positivity, except for the growth-rate parameter $\boldsymbol{\lambda}$ in the exponential model, which was estimated directly on its original scale. Models were fitted by maximum likelihood in R using the nlme package. The complete mathematical model formulations and estimation details are provided in the Supplementary Methods. Following model fitting, pairwise comparisons among the six gapmer–hormone conditions were performed for the relevant condition-specific parameters in each model, using estimated marginal means from the emmeans framework with Tukey adjustment for multiple comparisons.

For the other analyses, data are presented as mean ± SEM, or as normalized fold change ± SEM, as specified in the corresponding figure legends. The number of independent biological experiments and replicates is indicated in the figure legends. For experiments involving two experimental factors, including MALAT1 targeting (LacZ versus MALAT1 gapmers) and hormonal or pharmacological treatment, we analyzed data by two-way ANOVA followed by Bonferroni's multiple-comparisons test. For the PTGS2 co-targeting experiments, we analyzed data by three-way ANOVA, with gapmer treatment (LacZ versus MALAT1), PTGS2 silencing (NC1 versus siPTGS2), and hormonal treatment (vehicle, DHT, or E2) as experimental factors, followed by Bonferroni's multiple-comparisons test. Supplementary Figure S1B and S1C were analyzed using one-way ANOVA followed by Bonferroni's multiple-comparisons test. ANOVA-based analyses were performed using GraphPad Prism version 10.4.0. Statistical significance was defined as $p \leq 0.05$.

## 3. Results

### 3.1 MALAT1 Basal Expression Across Breast Cancer Cell Lines and Primary Cultures, and Targeting Efficiency

The study combined established *in vitro* models with patient-derived *ex vivo* cultures. MCF7 and T47D were used as ERα-positive HR+ breast cancer models, whereas LNCaP and 22RV1 provided hormone-responsive and hormone-refractory prostate cancer reference models, respectively. We generated six primary cultures from Luminal B tumors with heterogeneous ERα, PR, AR, and Ki67 profiles (Table 1). Western blotting and immunocytochemistry showed a prevalent luminal/epithelial phenotype, with ERα and AR expression, variable E-cadherin and vimentin, absent α-SMA, and heterogeneous cytokeratin positivity (Table 2).

Basal MALAT1 expression varied across breast epithelial and cancer-cell models (Supplementary Fig. S1A). T47D displayed the highest level among the established breast cancer lines tested, whereas HCC1806 and MDA-MB-231 showed lower expression. MALAT1 was detectable in all six Luminal B patient-derived cultures: ePG5, ePG9, ePG11, ePG25, ePG43, and ePG55.

LNA-GapmeR treatment produced robust MALAT1 depletion in MCF7 and T47D cells at 48 h and 72 h, in both complete medium and hormone-deprived conditions (Supplementary Fig. S1B). Efficient targeting was independently confirmed in ePG9, ePG11, ePG25, and ePG43 (Supplementary Fig. S1C). These data establish robust MALAT1 targeting in established HR+ lines and patient-derived cultures.

### 3.2 MALAT1 Depletion Exerts Cell-Context-Dependent Anti-Proliferative Effects

To compare MALAT1 dependence across hormone-responsive cancer contexts, LNCaP and 22RV1 prostate cancer cells and ERα-positive MCF7 and T47D breast cancer cells were transfected with LacZ or MALAT1 gapmer under hormone-deprived conditions, exposed to vehicle, DHT (10 nM), or E2 (10 nM), and monitored longitudinally by IncuCyte phase-object analysis for up to 7 days (Fig. 1, left panels).

To formally analyze the full-time course, we fitted longitudinal IncuCyte data using nonlinear mixed-effects growth models selected based on the observed kinetics of each cell line. We used exponential models for LNCaP and T47D, and Hill models for MCF7 and 22RV1. The models incorporated condition-specific fixed effects for the six gapmer-hormone combinations and experimental-unit-level random effects, thereby accounting for nonlinear growth behavior, repeated measurements, and between-experiment variability (Figure 1, right panels). Pairwise comparisons of condition-specific model parameters were performed using estimated marginal means with Tukey adjustment (Table 3). The nonlinear mixed-effects analysis demonstrated a clear cell-context dependence of the basal response to MALAT1 depletion. In MCF7 cells, MALAT1 targeting alone significantly reduced the fitted proliferation trajectory relative to LacZ vehicle (adjusted $p<0.0001$). By contrast, no significant difference between LacZ vehicle and MALAT1 vehicle was detected in T47D ($p=0.0945$), LNCaP ($p=0.3509$), or 22RV1 ($p=0.9974$). Thus, the anti-proliferative effect of MALAT1 targeting alone is not uniform across hormone-responsive cancer models and, among the breast cancer lines examined, is prominent in MCF7 but not in T47D cells.

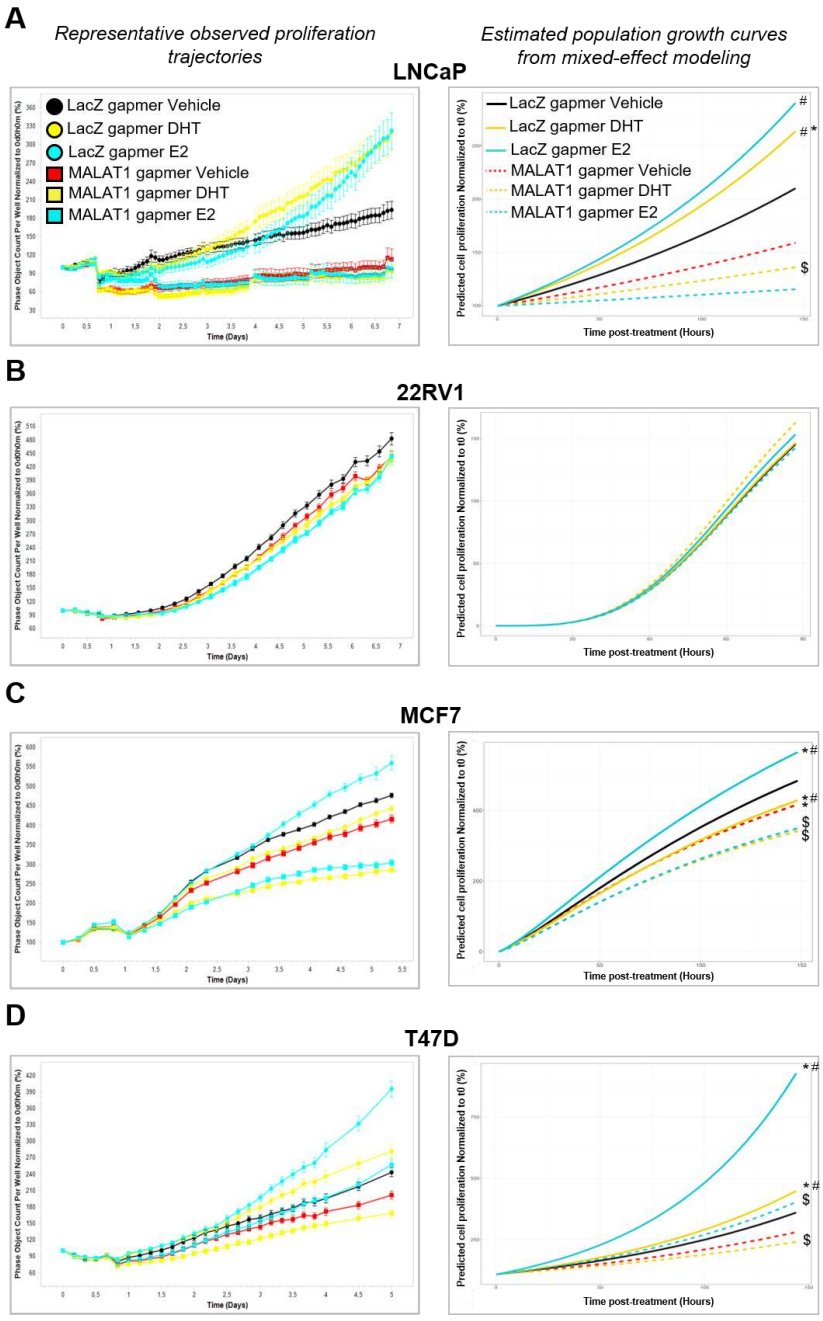



***Figure 1. MALAT1 depletion differentially modifies hormone-driven proliferation across cancer cell models.*** Cell proliferation was monitored under hormone-deprived conditions using the IncuCyte live-cell analysis system in (A) LNCaP, (B) 22RV1, (C) MCF7, and (D) T47D cells transfected with either a LacZ control gapmer or a MALAT1-targeting gapmer and treated approximately 16 h later with vehicle, DHT (10 nM), or E2 (10 nM). The left panels show representative observed proliferation trajectories from one independent experiment for each cell line; the right panels show population-level predicted proliferation trajectories for the six experimental conditions, obtained from cell-line-specific nonlinear mixed-effects growth models with random effects set to zero. The six modelled conditions were LacZ gapmer-vehicle,-DHT, or E2, and MALAT1 gapmer-vehicle, -DHT, or E2. Symbols denote statistically significant model-based pairwise comparisons: * P≤0.05, MALAT1-gapmer versus LacZ-gapmer within the same hormone condition; # P≤0.05, vehicle versus DHT or E2 within LacZ-gapmer conditions; $ P≤0.05, vehicle versus DHT or E2 within MALAT1-gapmer conditions. Pairwise comparisons were based on estimated marginal means with Tukey adjustment for multiple testing. Individual P-values are shown in Table 3.

*Table 3. Pairwise contrasts of condition-specific model parameters in immortalized cell lines*

| Pairwise contrast | Estimate | SE | df | t.ratio | p.value |
|---|---|---|---|---|---|
| **LNCaP** | | | | | |
| **LacZ gapmer Vehicle – MALAT1 gapmer Vehicle** | 0,001917 | 0,000965 | 658 | 1,987 | 0.3509 |
| **LacZ gapmer Vehicle - LacZ gapmer DHT** | -0,001556 | 0,000205 | 658 | -7,607 | **<0.0001** |
| **LacZ gapmer Vehicle - LacZ gapmer E2** | -0,002219 | 0,000551 | 658 | -4,027 | **0.0009** |
| **MALAT1 gapmer Vehicle - MALAT1_gapmer DHT** | 0,001067 | 0,000305 | 658 | 3,495 | **0.0067** |
| **MALAT1 gapmer Vehicle - MALAT1 gapmer E2** | 0,002194 | 0,00117 | 658 | 1,868 | 0.4232 |
| **LacZ gapmer DHT - MALAT1 gapmer_DHT** | 0,004541 | 0,00143 | 658 | 3,185 | **0.0188** |
| **LacZ gapmer E2 - MALAT1 gapmer E2** | 0,00633 | 0,00267 | 658 | 2,368 | 0.1690 |
| **22RV1** | | | | | |
| **LacZ gapmer Vehicle – MALAT1 gapmer Vehicle** | -0.007152 | 0.0156 | 189 | -0.459 | 0.9974 |
| **LacZ gapmer Vehicle - LacZ gapmer DHT** | -0.007505 | 0.0312 | 189 | -0.241 | 0.9999 |
| **LacZ gapmer Vehicle - LacZ gapmer E2** | -0.052573 | 0.0636 | 189 | -0.827 | 0.9623 |
| **MALAT1 gapmer Vehicle - MALAT1_gapmer DHT** | -0.105739 | 0.0397 | 189 | -2.662 | 0.0878 |
| **MALAT1 gapmer Vehicle - MALAT1 gapmer E2** | 0.026529 | 0.0730 | 189 | 0.364 | 0.9992 |
| **LacZ gapmer DHT - MALAT1 gapmer_DHT** | -0.105386 | 0.0313 | 189 | -3.366 | **0.0117** |
| **LacZ gapmer E2 - MALAT1 gapmer E2** | 0.071950 | 0.0336 | 189 | 2.139 | 0.2720 |
| **MCF7** | | | | | |
| **LacZ gapmer Vehicle – MALAT1 gapmer Vehicle** | 0.3054 | 0.0260 | 1273 | 11.758 | **<0.0001** |
| **LacZ gapmer Vehicle - LacZ gapmer DHT** | 0.2000 | 0.0299 | 1273 | 6.692 | **<0.0001** |
| **LacZ gapmer Vehicle - LacZ gapmer E2** | -0.1416 | 0.0255 | 1273 | -5.554 | **<0.0001** |
| **MALAT1 gapmer Vehicle - MALAT1_gapmer DHT** | 0.2544 | 0.0259 | 1273 | 9.828 | **<0.0001** |
| **MALAT1 gapmer Vehicle - MALAT1 gapmer E2** | 0.1866 | 0.0262 | 1273 | 7.113 | **<0.0001** |
| **LacZ gapmer DHT - MALAT1 gapmer_DHT** | 0.3599 | 0.0304 | 1273 | 11.854 | **<0.0001** |
| **LacZ gapmer E2 - MALAT1 gapmer E2** | 0.6336 | 0.0284 | 1273 | 22.279 | **<0.0001** |
| **T47D** | | | | | |
| **LacZ gapmer Vehicle – MALAT1 gapmer Vehicle** | 0.001742 | 0.000666 | 697 | 2.617 | 0.0945 |
| **LacZ gapmer Vehicle - LacZ gapmer DHT** | -0.001521 | 0.000528 | 697 | -2.879 | **0.0472** |
| **LacZ gapmer Vehicle - LacZ gapmer E2** | -0.006570 | 0.001430 | 697 | -4.598 | **<0.0001** |
| **MALAT1 gapmer Vehicle - MALAT1_gapmer DHT** | 0.001049 | 0.000365 | 697 | 2.876 | **0.0474** |
| **MALAT1 gapmer Vehicle - MALAT1 gapmer E2** | -0.002535 | 0.000361 | 697 | -7.025 | **<0.0001** |
| **LacZ gapmer DHT - MALAT1 gapmer_DHT** | 0.004313 | 0.000477 | 697 | 9.034 | **<0.0001** |
| **LacZ gapmer E2 - MALAT1 gapmer E2** | 0.005777 | 0.000868 | 697 | 6.658 | **<0.0001** |

Pairwise contrasts were calculated for the condition-specific λ parameter in LNCaP and T47D cell lines and for the condition-specific log(K) parameter in MCF7 and 22RV1 cell lines.

### 3.3 Combined MALAT1 Targeting + E2 Treatment Abolishes E2-Driven Proliferation and Reveals a Growth-Inhibitory Response in HR+ Breast Cancer Cells

The most distinctive biological finding emerged when HR+ breast cancer cells were exposed to E2 after MALAT1 targeting. Under hormone-deprived conditions, E2 significantly enhanced the fitted proliferation trajectory in LacZ-transfected MCF7 and T47D cells, confirming an intact estrogen-responsive mitogenic program. After MALAT1 depletion, however, E2 no longer sustained the same proliferative response.

Specifically, in **MCF7**, LacZ gapmer + E2 combination differed markedly from MALAT1 gapmer + E2 (adjusted p<0.0001), and MALAT1 gapmer + E2 trajectory was also significantly lower than the MALAT1 gapmer vehicle trajectory (p<0.0001). To directly test whether the effect of E2 differed between control and MALAT1-depleted cells, we calculated a planned difference-in-differences contrast on the estimated $\log K$values. The contrast was defined as $\Delta = [\log K_{\mathrm{LacZ+E2}} - \log K_{\mathrm{LacZ+vehicle}}] - [\log K_{\mathrm{MALAT1+E2}} - \log K_{\mathrm{MALAT1+vehicle}}]$. This interaction contrast was positive and significant ($\Delta = 0.328$, SE $= 0.0378$, 95% CI [0.254, 0.402], $p < 0.0001$). Thus, after MALAT1 depletion, the positive effect of E2 observed in control cells was reversed, with E2 instead being associated with a reduction in the asymptotic proliferation parameter. In T47D cells, MALAT1 targeting alone did not significantly affect basal proliferation. The MALAT1-gapmer + E2 trajectory was markedly lower than the LacZ-gapmer + E2 trajectory (p<0.0001) but remained significantly higher than the MALAT1-gapmer vehicle trajectory (p<0.0001). Therefore, E2 retained a mitogenic effect in MALAT1-depleted T47D cells, although this response was substantially attenuated. These findings distinguish a growth-inhibitory E2 response in MCF7 cells from a reduced but persistent E2-supported proliferative response in T47D cells.

DHT responses were also cell line-dependent. In MCF7 cells, LacZ-gapmer + DHT reduced the fitted trajectory relative to LacZ-gapmer vehicle (p<0.0001), and MALAT1-gapmer + DHT was lower than LacZ-gapmer + DHT (p<0.0001). In T47D cells, LacZ-gapmer + DHT modestly increased proliferation relative to LacZ-gapmer vehicle (p=0.0472), whereas MALAT1-gapmer + DHT produced a significantly lower trajectory than LacZ-gapmer + DHT (p<0.0001). These

divergent androgen responses further support cell-context-dependent integration of hormone signaling and MALAT1 function.

Overall, longitudinal analysis strengthens the central biological conclusion by distinguishing cell-line-specific basal MALAT1 dependence from hormone-dependent effects. MCF7 cells show a strong basal anti-proliferative response to MALAT1 targeting, whereas T47D cells do not; nevertheless, both lines show a highly significant loss of E2-supported proliferation after MALAT1 depletion. In the prostate cancer models, MALAT1 targeting alone did not significantly alter basal proliferation. LNCaP cells retained DHT responsiveness in LacZ-gapmer controls, whereas the MALAT1-gapmer + DHT trajectory was significantly lower than LacZ-gapmer + DHT ($p=0.0188$); 22RV1 cells showed negligible overall hormone responsiveness. Together, these results support a context-dependent role for MALAT1 in hormone-driven proliferation rather than a uniform growth requirement across tumor types.

### 3.4 Combined MALAT1 Targeting + E2 Treatment Is Associated with Loss of ME3 Hormone Responsiveness and Maximal PTGS2/COX-2 Induction

qRT-PCR profiling showed efficient MALAT1 knockdown in MCF7 and T47D under all treatment conditions (Fig. 2). The canonical hormone-responsive controls confirmed functional receptor signaling: E2 strongly induced *PS2/TFF1* (Fig. 2), whereas DHT induced *FKBP5* (Fig. 2), with cell-line-specific differences in magnitude.

In prostate cancer, MALAT1 depletion strongly represses *ME3* and pyruvate dehydrogenase kinase genes (*PDKs*), identifying a MALAT1-dependent metabolic transcriptional program [11]. Transcriptomic analysis of MALAT1-deficient TNBC models has likewise demonstrated broad reprogramming of oxidative phosphorylation and survival networks [10]. We therefore tested whether the ME3/PDK3 metabolic axis was conserved in HR+ breast cancer, contributing to the marked growth-inhibitory phenotype and extending the analysis to PTGS2/COX-2 as a potential adaptive inflammatory-survival response.

*PDK3* was modestly reduced by MALAT1 targeting in MCF7 and remained largely unchanged in T47D (Fig. 2). Notably, In LacZ controls, E2 significantly induced *ME3*; after MALAT1 targeting, basal *ME3* expression was reduced, and its E2 response remained markedly lower than in E2-treated controls (Fig. 2). Conversely, *PTGS2*/COX-2 reached its highest levels under combined

MALAT1 targeting + E2 treatment in both cell lines (Fig. 2). Thus, the experimental condition associated with growth suppression was also characterized by impaired ME3 responsiveness and maximal induction of the COX-2 pathway. Additional qRT-PCR analyses of *ESR1/ERα*, *AR*, *ME1*, *ME2*, and *CCND1* showed comparatively modest or context-dependent changes and are presented in Supplementary Figure S2.

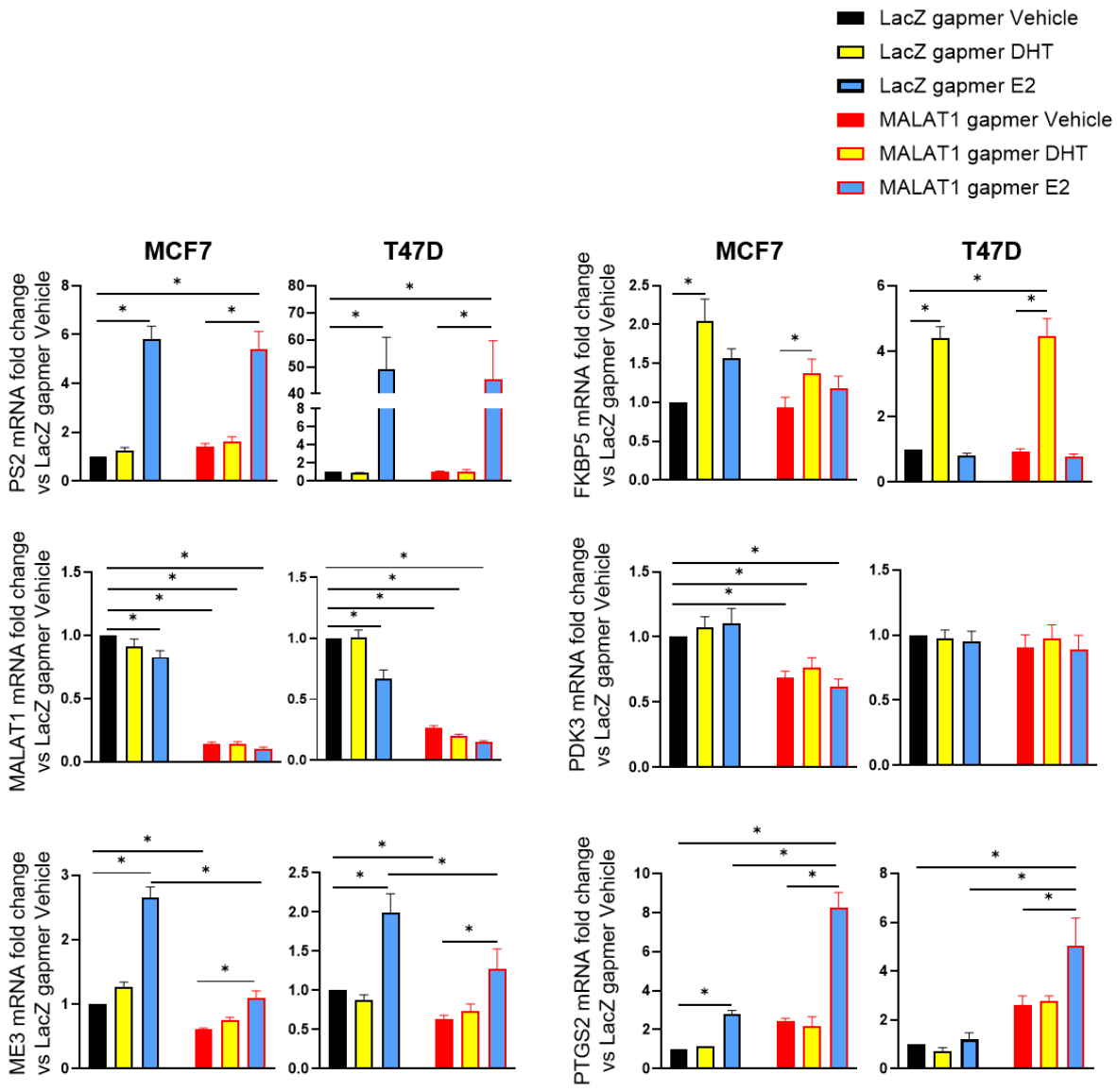



***Figure 2. MALAT1 depletion impairs ME3 responsiveness and enhances E2-associated PTGS2/COX-2 induction.*** qRT-PCR analysis of MALAT1, PS2/TFF1, FKBP5, PDK3, ME3, and PTGS2 mRNA levels in MCF7 and T47D cells transfected with LacZ control or MALAT1-targeting gapmer and exposed to vehicle, DHT (10 nM), or E2 (10 nM). Cells were harvested 72 h after gapmer transfection, following 48 h of hormone treatment. Values are fold changes relative to LacZ-gapmer vehicle and are shown as mean ± SEM from four independent biological experiments. * P≤0.05.

Representative immunoblots provided supportive protein-level evidence (Supplementary Fig. S3). ME3 tended to decrease after MALAT1 depletion +E2, particularly in MCF7, whereas COX-2 tended to increase, with the most evident induction in hormone-treated MALAT1-depleted cells. ERα and AR protein abundance also changed across conditions, but the patterns were not uniform between MCF7 and T47D. These protein data are therefore interpreted as directional support for the transcriptional changes rather than as a fully quantitative endpoint.

### 3.5 Combined MALAT1 Targeting + E2 Treatment Maximally Activates COX-2 in MCF7 and Engages an Inflammatory-Stress and Cell-Death Response

We next investigated whether the molecular profile associated with the growth-inhibitory response to combined MALAT1 targeting + E2 treatment was accompanied by functional COX-2 activation and inflammatory-stress or cell-death signals (Fig. 3).

*PTGS2*/COX-2 links estrogen signaling with prostaglandin production, oxidative stress responses, and cancer cell survival, whereas IL-6 and CASP8 provide complementary readouts of inflammatory and cell-death programs. Because MALAT1 loss can broadly reprogram metabolic and inflammatory pathways [10,29], we tested whether the transcript-level PTGS2 increase was accompanied by COX-2 enzymatic activation and induction of IL-6, CASP8, and Annexin V.

We measured COX-2 activity in MCF7 and T47D cells after LacZ or MALAT1 gapmer treatment, with or without E2. In MCF7 cells, analysis of three independent experiments showed that E2 significantly increased COX-2 activity. The highest activity was observed with MALAT1 targeting + E2 treatment and was significantly higher than both the vehicle control and MALAT1 targeting alone (Fig. 3A). T47D cells showed the same directional trend, but variability was greater, and the comparisons did not reach statistical significance.

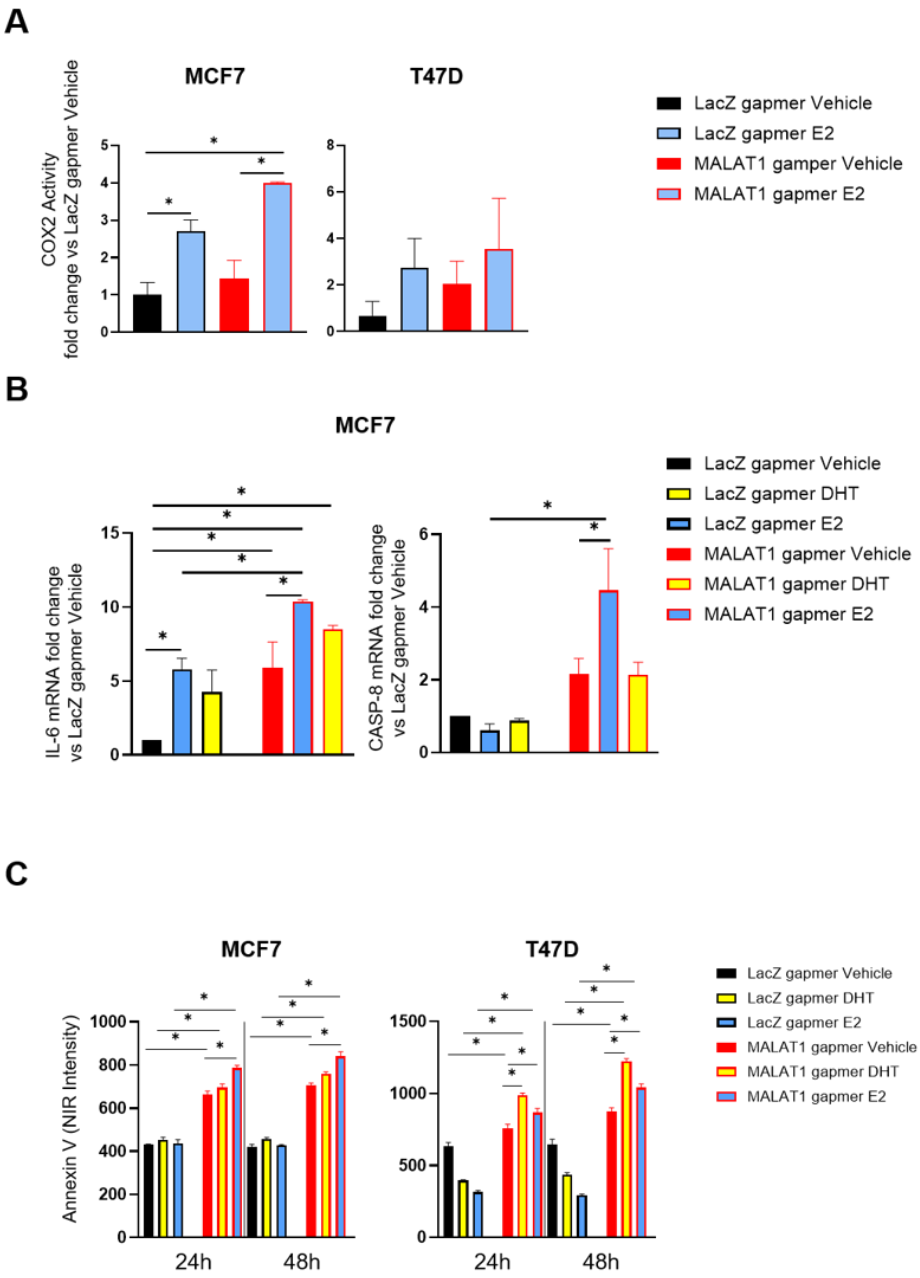



***Figure 3. Combined MALAT1 targeting and E2 exposure activates COX-2 and is associated with inflammatory-stress and cell-death signals.*** (A) COX-2 enzymatic activity in MCF7 (left) and T47D (right) after LacZ control or MALAT1-targeting gapmer transfection (72 h) and treatment with vehicle or E2 (10 nM, 48 h). Data are expressed as fold change relative to LacZ-gapmer vehicle and are shown as mean ± SEM from three independent biological experiments. (B) qRT-PCR analysis of IL6 and CASP8 mRNA expression in MCF7 cells after LacZ or MALAT1 gapmer transfection (72 h) and treatment with vehicle, DHT (10 nM, 48 h), or E2 (10 nM, 48 h). Expression is reported as fold change relative to LacZ-gapmer vehicle and shown as mean ± SEM from three independent biological experiments. (C) Analysis at 24 h and 48 h of Annexin V labeling [NIR Integrated Intensity Object Average normalized to 2 days 18 hours (%)] in MCF7 and T47D cells transfected with LacZ or MALAT1 gapmers (16 h) and subsequently treated with vehicle, DHT (10 nM), or E2 (10 nM). Expression is reported as mean ± SEM from three independent experiments. * P≤0.05.

In addition, we analyzed *IL-6* and *CASP8* transcripts in MCF7 cells under vehicle, E2, and DHT conditions. Although the *IL-6* transcript increased after MALAT1 targeting, both *IL-6* and *CASP8* mRNAs peaked under combined MALAT1 targeting + E2 treatment (Fig. 3B). This co-induction is consistent with activation of a stress-associated inflammatory program.

Annexin V NIR intensity was higher in MALAT1-targeted cultures than in LacZ controls (Fig. 3C). In hormone-treated MALAT1-targeted cells, the strongest Annexin V response occurred at 24 h and 48 h time points. Collectively, the data link loss of E2-driven proliferation to COX-2 activation, IL-6/CASP8 induction, and increased cell-death signaling.

### 3.6 MALAT1 Targeting Remodels ERα and AR Recruitment at PTGS2 and PS2 promoters and Alters PTGS2 Regulation in a Cell-Line-Dependent Manner

To assess whether MALAT1 targeting altered hormone-receptor recruitment, ChIP assays were performed for ERα and AR in hormone-deprived MCF7 and T47D cells transfected with LacZ or MALAT1 gapmers and treated with vehicle or E2 (Fig. 4A). The main figure focuses on the *PTGS2* promoter (encompassing the ER-Sp1 binding site as described in [30]) and the estrogen-responsive *PS2/TFF1* promoter.

In MCF7 cells, E2 increased ERα occupancy at the *PTGS2* and *PS2* genes in LacZ controls, whereas MALAT1 targeting markedly reduced this recruitment. AR showed the reciprocal pattern: E2 reduced AR occupancy at *PTGS2* in control cells, while combined MALAT1 targeting + E2 treatment produced strong AR enrichment at both *PTGS2* and *PS2* promoters. T47D showed a different pattern, with increased recruitment of both ERα and AR after MALAT1 targeting + E2 at the PTGS2 promoter; in parallel, MALAT1 targeting alone showed stronger ERα and AR occupancy at the PS2 promoter. Thus, the data support receptor redistribution in MCF7 but concurrent receptor recruitment in T47D rather than a universal ERα-to-AR switch.

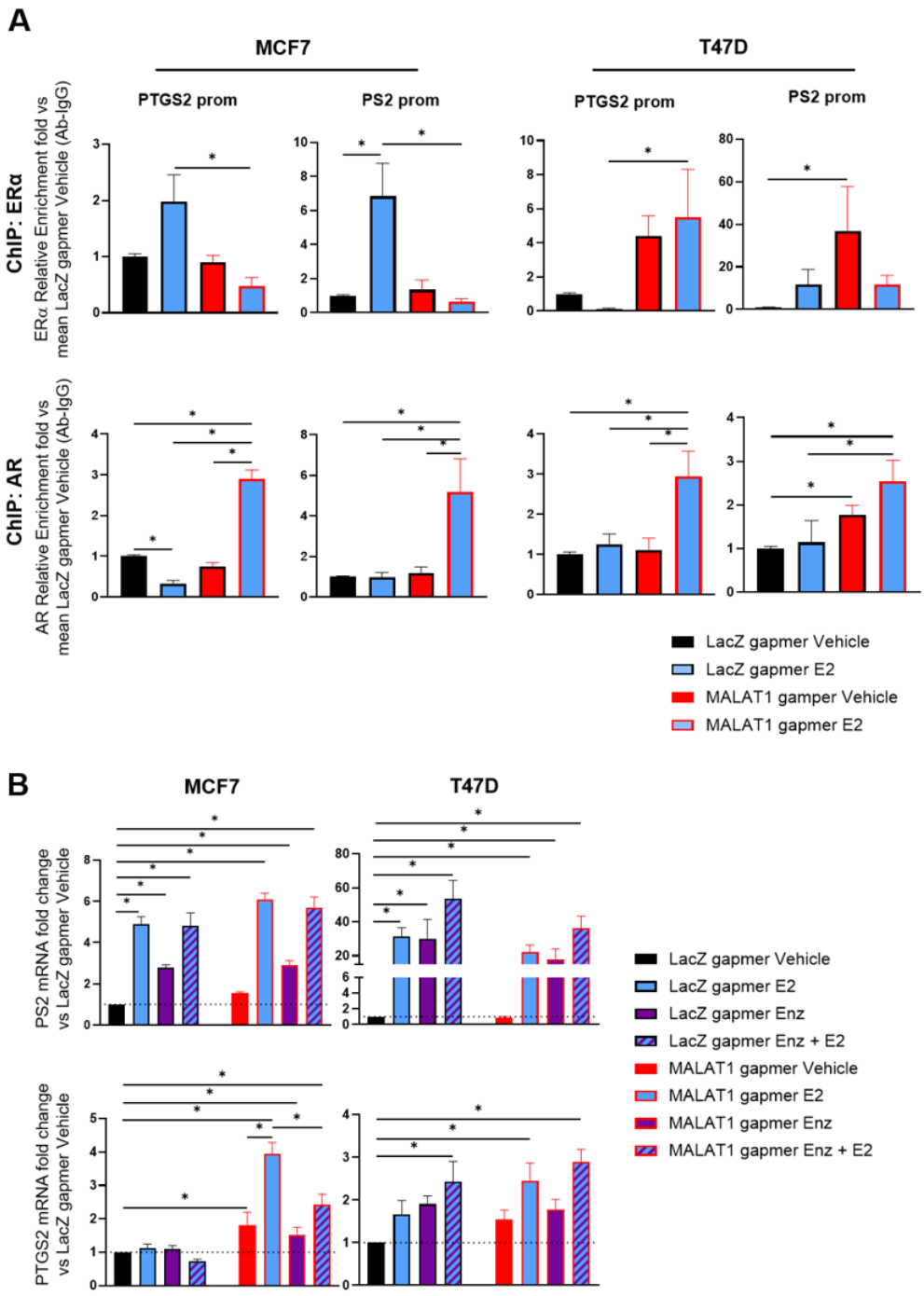



***Figure 4. MALAT1 depletion remodels ERα and AR occupancy at PTGS2 and PS2/TFF1 promoters in a cell-line-dependent manner.*** (A) ChIP-qPCR analysis of ERα (upper panels) and AR (lower panels) occupancy at the PTGS2 and PS2/TFF1 promoters in MCF7 and T47D cells transfected for 48 h with LacZ control or MALAT1-targeting gapmer and subsequently exposed to vehicle or E2 (100 nM, 45 min). IgG served as a negative control. Data are expressed as fold enrichment relative to the mean LacZ-gapmer vehicle condition after subtraction of IgG ± SEM from three independent biological experiments. (B) qRT-PCR analysis of PS2/TFF1 and PTGS2 mRNA levels in MCF7 and T47D cells following LacZ or MALAT1 gapmer transfection (72 h) and treatment with vehicle, E2 (10 nM, 48 h), enzalutamide (ENZ;10 μM, 48 h), or ENZ + E2. Expression is reported as fold change relative to LacZ-gapmer vehicle and shown as mean ± SEM from three independent biological experiments. * P≤0.05.

Functional qRT-PCR after E2, enzalutamide (ENZ), or ENZ + E2 treatment supported this cell-line distinction (Fig. 4B). Of note, enzalutamide was used to abrogate AR signaling by impairing AR nuclear translocation. ENZ significantly attenuated *PTGS2* induction under combined MALAT1 targeting + E2 treatment in MCF7, supporting an AR contribution, but did not produce an analogous reduction in T47D. Supplementary Figure S4 extends the analysis to the *ME3* promoter (encompassing the androgen receptor site as described in [31]): MCF7 again showed lower ERα and higher AR occupancy in the combined condition, whereas T47D showed recruitment of both receptors. *ME3* expression decreased after MALAT1 targeting; E2 partially restored it, and it was reduced compared to E2, as shown in Figure 2, and ENZ did not produce a consistent rescue, indicating locus-specific receptor remodeling without a simple fixed activating or repressive effect.

### 3.7 PTGS2/COX-2 Depletion Increases Cell-Death Susceptibility after MALAT1 Targeting in Selected Conditions

Induction of *PTGS2*/COX-2 after MALAT1 targeting suggested that COX-2 might contribute to adaptation to MALAT1-dependent stress. MCF7 and T47D cells were therefore co-transfected with LacZ or MALAT1 gapmers and either *PTGS2*-targeting siRNA or the NC1 control under vehicle, DHT, or E2 conditions. qRT-PCR confirmed persistent MALAT1 depletion and effective *PTGS2* reduction while documenting *PS2*, *FKBP5*, and *ME3* responses (Supplementary Fig. S5). Dead cell values are shown in Figure 5. In T47D, MALAT1 targeting increased cell death, and siPTGS2 maintained cell death under vehicle and E2 conditions. In MCF7, siPTGS2 showed an additional effect only under combined MALAT1 targeting and hormonal treatment. These data support a context-dependent contribution of COX-2 to survival after MALAT1 targeting, without establishing formal synthetic lethality.

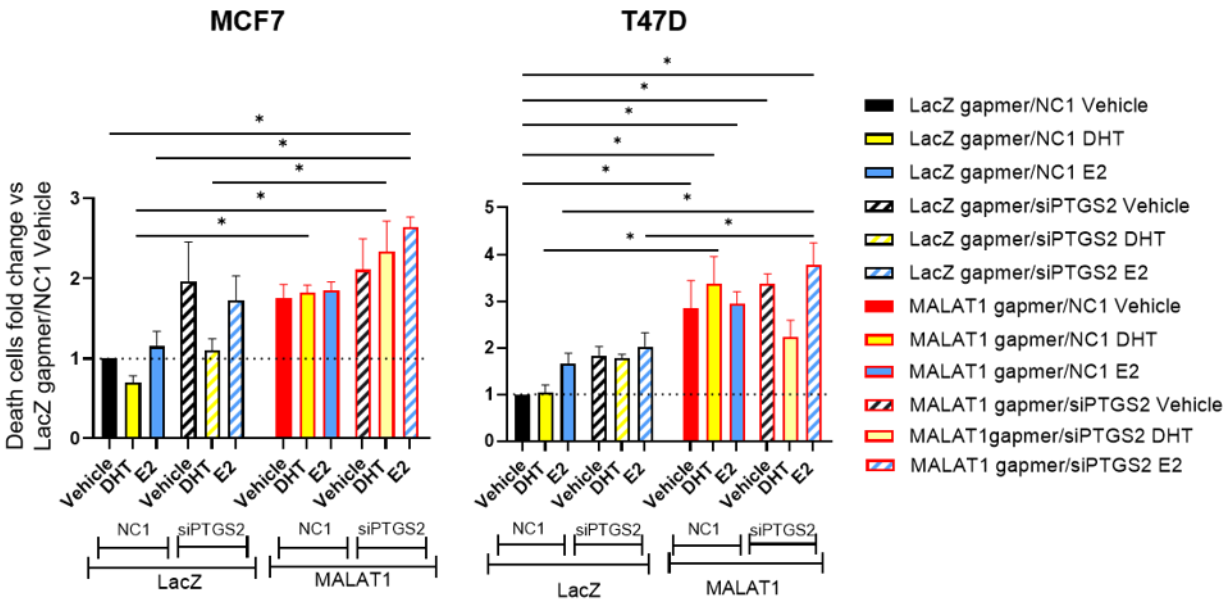



***Figure 5. PTGS2 depletion increases cell-death susceptibility after MALAT1 targeting in selected conditions.*** Dead-cell measurements in MCF7 (left) and T47D (right) cells co-transfected with LacZ control or MALAT1-targeting gapmer (72 h) and either non-targeting NC1 siRNA or PTGS2-targeting siRNA. Cells were analyzed after 72 h of gapmer/siRNA treatment under vehicle, DHT (10 nM, 48 h), or E2 (10 nM, 48 h) conditions. Within each LacZ- or MALAT1-gapmer group, solid bars represent NC1-transfected cells and hatched bars represent PTGS2-silenced cells. Dead-cell values are expressed as fold change relative to LacZ gapmer/NC1 vehicle condition and are presented as mean ± SEM from three independent biological experiments. * P≤0.05.

### 3.9 MALAT1 Depletion Abolishes E2-Dependent Growth and Enhances Annexin V Signal in Primary Breast Cancer Cultures

The six primary cultures originated from Luminal B tumors spanning 39-65 years of age, including five invasive ductal carcinomas and one invasive lobular carcinoma. The original biopsies displayed broad ERα (40-95%), PR (<1-90%), AR (30-95%), and Ki67 (22-65%) expression ranges (Table 1), while the derived cultures retained a prevalent but heterogeneous luminal/epithelial phenotype (Table 2 and Supplementary Fig. S6A and B). We functionally evaluated five cultures (ePG5, ePG9, ePG11, ePG43, and ePG55) by IncuCyte (Fig. 6).

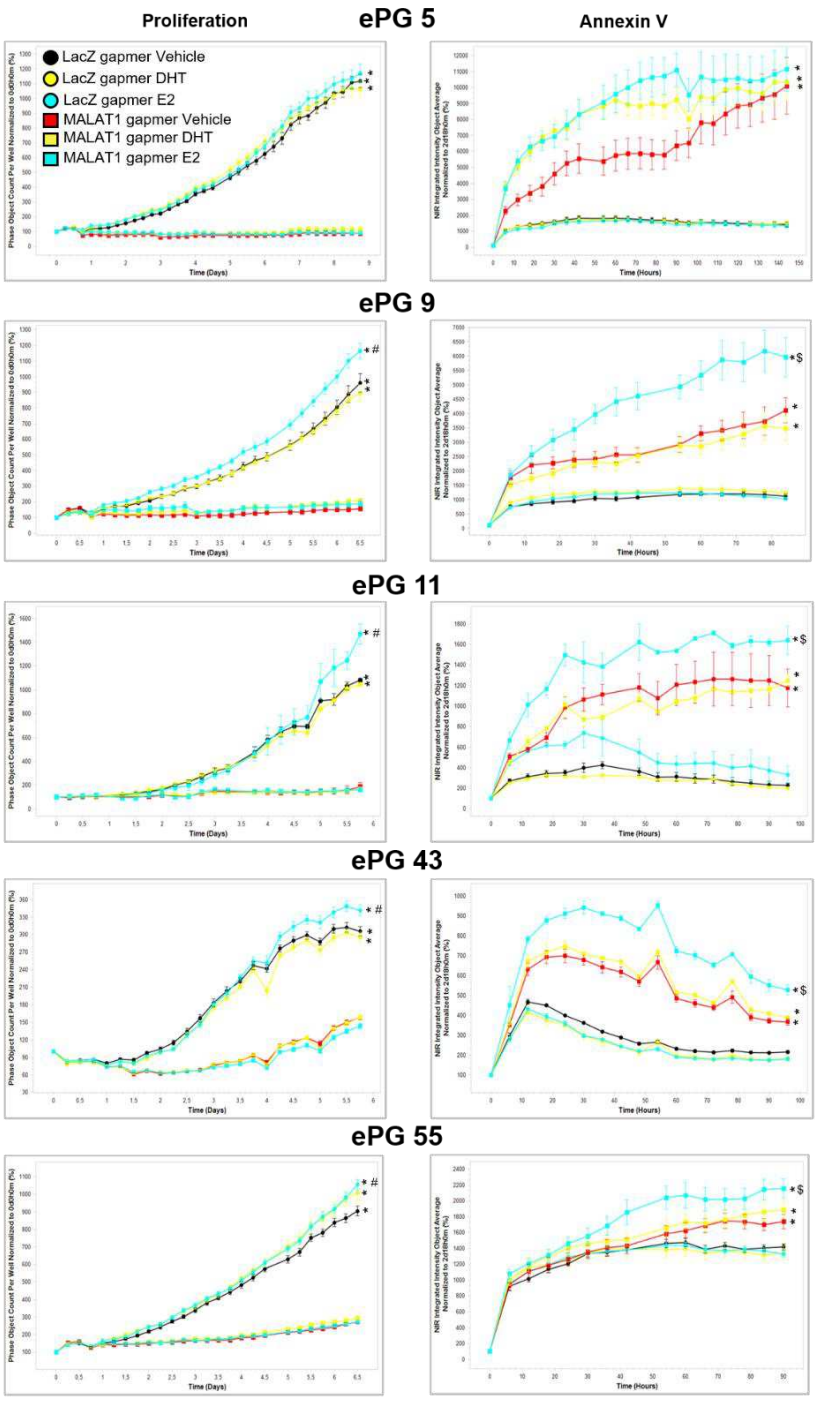



***Figure 6. Combined MALAT1 targeting + E2 treatment abolishes E2-supported growth and frequently enhances Annexin V signal in primary breast cancer cultures.*** IncuCyte analysis of five patient-derived Luminal B breast cancer cultures (ePG5, ePG9, ePG11, ePG43, and ePG55) following LacZ control or MALAT1-targeting gapmer transfection (16 h) and treatment with vehicle, DHT (10 nM), or E2 (10 nM). For each primary culture, the left panel shows cell-proliferation kinetics, and the right panel shows the corresponding Annexin V NIR cell-death kinetics. The figure shows one representative experiment from two independent biological experiments. We performed statistical analysis at the last time-point of each cell culture. * P≤0.05, MALAT1-gapmer versus LacZ-gapmer within the same hormone condition; # P≤0.05, vehicle versus DHT or E2 within LacZ-gapmer conditions; $ P≤0.05, vehicle versus DHT or E2 within MALAT1-gapmer conditions.

In LacZ controls, E2 increased proliferation relative to vehicles in 4 of 5 primary cultures, demonstrating preserved estrogen responsiveness. MALAT1 targeting markedly reduced proliferation in all five cultures, and E2-treated MALAT1-targeted cells remained strongly growth-suppressed. Combined MALAT1 targeting + E2 treatment produced a significant increase in Annexin V signal, particularly in ePG9, ePG11, ePG43, and ePG55. DHT responses were more variable.

Molecular analysis of representative ePG9 and ePG11 cultures supported the cell-line findings (Supplementary Fig. S6C). MALAT1 targeting reduced MALAT1 expression to less than 5% of the corresponding LacZ control under vehicle, DHT, and E2 conditions, and reduced ME3 mRNA levels by approximately 70-80%. In contrast, *PTGS2* mRNA level increased approximately 2.5- to 3-fold after MALAT1 targeting, with a further increase under combined MALAT1 targeting + E2 treatment. Overall, these results demonstrate that the loss of estrogen-supported growth after MALAT1 targeting is reproducible across patient-derived models.

## 4. Discussion

This study examines how MALAT1 depletion alters the biological response to estrogen in HR+ breast cancer cells. E2 served as a mitogenic stimulus in LacZ-gapmer controls in both MCF7 and T47D cells, but MALAT1 depletion had different effects in the two models. In MCF7 cells, combining MALAT1 targeting with E2 exposure reduced proliferation below that of the MALAT1-gapmer vehicle, revealing a growth-inhibitory response. In T47D cells, E2 still increased proliferation relative to the MALAT1-gapmer vehicle, though the response was markedly weaker than in LacZ-gapmer controls. Thus, MALAT1 contributes to the full proliferative action of E2 in both cell lines, but a complete conversion to a growth-inhibitory phenotype was observed only in MCF7 cells. This distinction is central to interpreting the study and underscores the context dependence of MALAT1 function in HR+ breast cancer.

Although each primary culture could be experimentally tested only twice because of its limited lifespan, the relevance of combined MALAT1 targeting + E2 treatment is strengthened by its reproducibility across five independent primary cultures derived from clinically heterogeneous Luminal B tumors (Tables 1 and 2).

The primary-culture qRT-PCR data provide an additional layer of validation: MALAT1 targeting produced robust MALAT1 depletion and ME3 suppression, along with significant *PTGS2* induction, which was greatest under combined MALAT1 targeting + E2 treatment. ME3 reduction and *PTGS2*/COX-2 induction should therefore be interpreted as candidate mechanisms associated with a reproducible loss of estrogen-supported growth and induction of cell death, rather than as isolated findings. In line with this hypothesis, our data highlighted a pro-apoptotic role of COX-2 under MALAT1 targeting +E2 conditions, in agreement with previous results [32–34], although several studies reported an anti-apoptotic role of the COX-2 pathway [35–37]. Further studies are needed to clarify whether COX-2 upregulation under MALAT1 targeting + E2 treatment contributes to therapy resistance and immune escape [38–40]. Evidence from TNBC likewise indicates that MALAT1 can support persistence during neoadjuvant chemotherapy and that its deletion increases sensitivity to paclitaxel and doxorubicin while remodeling metabolic and inflammatory networks [10].

The prostate cancer comparison further illustrates this scenario. In the longitudinal models, MALAT1 targeting alone did not significantly alter basal proliferation in either LNCaP or in 22RV1 cells. LNCaP nevertheless retained a hormone-responsive phenotype, with significant DHT stimulation in LacZ gapmer controls and a significant inhibition in MALAT1 gapmer + DHT compared to LacZ gapmer + DHT. Whereas, 22RV1, as expected, exhibited virtually no hormone responsiveness. In contrast, DHT exerts cell-type specific effects on cell proliferation in breast cancer, reducing the growth rate in MCF7 cells while enhancing proliferation in T47D, likely due to the different AR/ERα ratio as compared to MCF7 cells. MALAT1 targeting + DHT combination exhibits in fact the lowest trajectory in both breast cancer cell lines. This context-specific behavior substantially aligns with recent evidence demonstrating that the absolute and relative abundance of AR and ERα dictates the biological outcome of AR signaling in hormone positive breast cancer [41,42]. Together, these observations argue against a simple prostate-versus-breast dichotomy and suggest that MALAT1 dependency is shaped by receptor composition, including the ER/AR balance, molecular subtype, transcriptional state, and treatment context. Crucially, our findings expand this paradigm by suggesting that MALAT1 depletion might actively modulate or intersect with this AR/ER ratio-dependent axis, potentially altering how breast and prostate cells perceive androgenic stimuli and reshuffling the chromatin binding dynamics of both receptors.

In line with this, the ChIP and enzalutamide results provide a candidate mechanism but require nuanced interpretation. In MCF7, combined MALAT1 targeting + E2 treatment was associated with reduced ERα and increased AR recruitment at *PTGS2* and *PS2* promoters (Fig. 4); therefore, ENZ partially reduced *PTGS2* induction. This reciprocal pattern is consistent with receptor redistribution at selected loci, but it does not establish that MALAT1 directly scaffolds ERα or excludes AR from chromatin. T47D instead showed concurrent ERα and AR recruitment under combined MALAT1 targeting + E2 treatment, attenuating AR's role in PTGS2 regulation, as shown by the absence of comparable ENZ-dependent suppression of *PTGS2*.

The *ME3* analysis in Supplementary Figure S4 further defines the limits of the model: MCF7 showed reciprocal ERα loss and AR gain under combined MALAT1 targeting + E2 treatment, whereas T47D showed recruitment of both receptors, and ENZ did not consistently restore *ME3* expression. Together, these findings support dynamic, locus- and cell-line-specific reorganization of receptor-containing chromatin complexes.

*ME3* reduction was among the most reproducible molecular effects of MALAT1 depletion. Because ME3 contributes to mitochondrial NADPH production, this observation suggests a potential redox and metabolic vulnerability [24,25,43]. However, the current study did not directly measure NADPH, glutathione status, or reactive oxygen species; oxidative stress should therefore be considered a mechanistic hypothesis rather than a demonstrated endpoint. *PTGS2* induction, increased COX-2 activity in MCF7, and *IL-6/CASP8* upregulation are consistent with an adaptive inflammatory-stress response. IL-6 induction alone does not establish cellular senescence or a complete SASP.

The *PTGS2* knockdown experiments indicate that COX-2 contributes to survival after MALAT1 targeting, but the effect is conditional. We consistently observed additional cell death in MCF7, particularly with E2, whereas no enhancement occurred in T47D, likely linked to parallel ME3 induction upon *siPTGS2* knockdown (Figure S5). These data reveal a dual role of COX-2 in determining survival or cell death depending on cell context, receptor composition, and MALAT1 targeting. Our data suggest the selective use of COX-2 silencing in combination with MALAT1 targeting, consistent with results observed in a clinical trial (ClinicalTrials.gov identifier: NCT01150045), in which a COX-2 inhibitor showed efficacy only in a subset of patients,

specifically those with a PIK3CA gain-of-function mutation or with ctDNA positivity in colorectal cancer ([44,45], respectively).

Several limitations should guide future work. The ChIP datasets should be expanded to include additional occupancy measurements at other loci. Direct quantification of NADPH, ROS, and prostaglandin levels, alongside caspase cleavage assays, would clarify the mechanistic links between ME3 deficiency, downstream inflammatory signaling, and compromised cell viability. Finally, the heterogeneous receptor and epithelial-marker profiles of the primary cultures, along with the absence of *in viv*o validation, currently limit translational generalization.

## 5. Conclusions

MALAT1 is required for estradiol to sustain a mitogenic response in MCF7 and T47D breast cancer cells and in multiple primary breast cancer cultures. Longitudinal nonlinear mixed-effects analysis showed that MALAT1 targeting alone strongly inhibits proliferation in MCF7 but not in T47D, LNCaP, or 22RV1 cells, while loss of E2-supported proliferation after MALAT1 depletion is highly significant in both HR+ breast cancer lines. This phenotype is associated with ME3 suppression, PTGS2/COX-2 induction and enzymatic activity, and cell-line- and locus-specific remodeling of ERα and AR chromatin occupancy. PTGS2 knockdown increases susceptibility to cell death under selected MALAT1-targeted conditions, suggesting a context-dependent contribution of COX-2 to survival. Together with the reproducibility of the phenotype across five patient-derived Luminal B cultures, these findings identify MALAT1 as a permissive regulator of estrogen-driven proliferation and nominate the MALAT1-ME3-COX-2 axis for further mechanistic, pharmacological, and in vivo investigation.

**Authors' contributions**. SDM designed the research, conducted experiments, collected and analyzed data, and performed statistical analyses. AA, VB, LC, MB, and RB conducted experiments. VP and SA contributed to data analysis and interpretation and revised the manuscript. AS evaluated and supervised IHC experiments. AFr, GF, and AF provided reagents and resources. SP performed longitudinal growth modeling using nonlinear mixed-effects growth modeling, revised the manuscript, and acquired funding. MP and ADG provided intellectual contribution and revised the formal analysis (nonlinear mixed-effects growth modeling) and manuscript. CG revised experimental data and the manuscript and acquired funding. SN revised experimental data and statistical analysis, acquired funding, and wrote and revised the manuscript. AFa designed the research, developed project conception, acquired funding, wrote the original draft, supervised, and revised the manuscript.

**Acknowledgements.** Authors are grateful to Alfredo Pontecorvi, department chair who provided general support. We thank the PhD School of Science of Nutrition, Metabolism, Aging and gender at Università Cattolica del Sacro Cuore, Rome, Italy, for VB and MB's PhD professional training.

**Funding:** The present study was supported by EU funding within the MUR PNRR "National Center for Gene Therapy and Drugs based on RNA Technology" (Project no. CN00000041, CN3 RNA) provided to AFa. The doctoral fellowship awarded to V.B. was funded by the Italian Ministry of University and Research (MUR), XXXVIII cycle, through the same PNRR CN3 program; and by MUR $D^3$4 Health - Digital Driven Diagnostics, prognostics and therapeutics for sustainable Health care (Project no. PNC0000001) - National Plan for NRRP Complementary Investments - Law Decree May 6, 2021, n. 59, converted and modified as to Law n. 101/2021 Research initiatives for technologies and innovative trajectories in the health and care sectors provided to SP.; Next Generation UE – PNRR M6C2 – Investimento 2.1 Valorizzazione e potenziamento della ricerca biomedica SSN (PNRR-POC-2023-12376976) to CG. CG is also supported by COST Action SENESCENCE2030, CA23119, supported by COST (European Cooperation in Science and Technology). AIRC also supported SN under IG 2019-ID 22858.

**Conflicts of Interest:** The authors declare no conflict of interest.

**Data Availability:** All raw data generated in this study are available from the corresponding author upon reasonable request.

## REFERENCES


1. Bray, F. *et al.* Global cancer statistics 2022: GLOBOCAN estimates of incidence and mortality worldwide for 36 cancers in 185 countries. *CA Cancer J Clin* **74**, 229–263 (2024).
2. Waks, A. G. & Winer, E. P. Breast Cancer Treatment: A Review. *JAMA* **321**, 288–300 (2019).
3. Statello, L., Guo, C.-J., Chen, L.-L. & Huarte, M. Gene regulation by long non-coding RNAs and its biological functions. *Nat Rev Mol Cell Biol* **22**, 96–118 (2021).
4. Ji, P. *et al.* MALAT-1, a novel noncoding RNA, and thymosin beta4 predict metastasis and survival in early-stage non-small cell lung cancer. *Oncogene* **22**, 8031–8041 (2003).
5. Bitaraf, A. *et al.* MALAT1 as a molecular driver of tumor progression, immune evasion, and resistance to therapy. *Mol Cancer* **24**, 245 (2025).
6. Kumar, D. *et al.* LncRNA Malat1 suppresses pyroptosis and T cell-mediated killing of incipient metastatic cells. *Nat Cancer* **5**, 262–282 (2024).
7. Barbi, V. *et al.* Non-coding RNAs as novel biomarkers and therapeutic targets in breast cancer. *Oncol Rev* **19**, 1621144 (2025).
8. Hussain, M. S. *et al.* Beyond the Genome: Deciphering the Role of MALAT1 in Breast Cancer Progression. *Curr Genomics* **25**, 343–357 (2024).
9. Kim, J. *et al.* Long noncoding RNA MALAT1 suppresses breast cancer metastasis. *Nat Genet* **50**, 1705–1715 (2018).
10. Shaath, H., Vishnubalaji, R., Elango, R., Khattak, S. & Alajez, N. M. Single-cell long noncoding RNA (lncRNA) transcriptome implicates MALAT1 in triple-negative breast cancer (TNBC) resistance to neoadjuvant chemotherapy. *Cell Death Discov* **7**, 23 (2021).

11. Nanni, S. *et al.* Metabolic Reprogramming by Malat1 Depletion in Prostate Cancer. *Cancers (Basel)* **13**, 15 (2020).
12. De Martino, S. *et al.* MALAT1 as a Regulator of the Androgen-Dependent Choline Kinase A Gene in the Metabolic Rewiring of Prostate Cancer. *Cancers (Basel)* **14**, 2902 (2022).
13. Leav, I. *et al.* Comparative studies of the estrogen receptors beta and alpha and the androgen receptor in normal human prostate glands, dysplasia, and in primary and metastatic carcinoma. *Am J Pathol* **159**, 79–92 (2001).
14. Hickey, T. E. *et al.* The androgen receptor is a tumor suppressor in estrogen receptor-positive breast cancer. *Nat Med* **27**, 310–320 (2021).
15. Smith, W. L., DeWitt, D. L. & Garavito, R. M. Cyclooxygenases: structural, cellular, and molecular biology. *Annu Rev Biochem* **69**, 145–182 (2000).
16. Wang, D. & Dubois, R. N. Prostaglandins and cancer. *Gut* **55**, 115–122 (2006).
17. Greenhough, A. *et al.* The COX-2/PGE2 pathway: key roles in the hallmarks of cancer and adaptation to the tumour microenvironment. *Carcinogenesis* **30**, 377–386 (2009).
18. Ristimäki, A. *et al.* Prognostic significance of elevated cyclooxygenase-2 expression in breast cancer. *Cancer Res* **62**, 632–635 (2002).
19. DE Cremoux, P. *et al.* COX2/PTGS2 Expression Is Predictive of Response to Neoadjuvant Celecoxib in HER2-negative Breast Cancer Patients. *Anticancer Res* **38**, 1485–1490 (2018).
20. Wu, C.-H. *et al.* Estradiol induces cell proliferation in MCF-7 mammospheres through HER2/COX-2. *Mol Med Rep* **19**, 2341–2349 (2019).
21. Tamura, M., Deb, S., Sebastian, S., Okamura, K. & Bulun, S. E. Estrogen up-regulates cyclooxygenase-2 via estrogen receptor in human uterine microvascular endothelial cells. *Fertil Steril* **81**, 1351–1356 (2004).

22. Loeber, G., Maurer-Fogy, I. & Schwendenwein, R. Purification, cDNA cloning and heterologous expression of the human mitochondrial NADP(+)-dependent malic enzyme. *Biochem J* **304 ( Pt 3)**, 687–692 (1994).
23. Murai, S. *et al.* Inhibition of malic enzyme 1 disrupts cellular metabolism and leads to vulnerability in cancer cells in glucose-restricted conditions. *Oncogenesis* **6**, e329 (2017).
24. Dey, P. *et al.* Genomic deletion of malic enzyme 2 confers collateral lethality in pancreatic cancer. *Nature* **542**, 119–123 (2017).
25. Chen, K.-C. *et al.* Targeting human mitochondrial NAD(P)+-dependent malic enzyme (ME2) impairs energy metabolism and redox state and exhibits antileukemic activity in acute myeloid leukemia. *Cell Oncol (Dordr)* **46**, 1301–1316 (2023).
26. Aiello, A. *et al.* MALAT1 and HOTAIR Long Non-Coding RNAs Play Opposite Role in Estrogen-Mediated Transcriptional Regulation in Prostate Cancer Cells. *Sci Rep* **6**, 38414 (2016).
27. Pecci, V. *et al.* A Feasibility Study of Co-Established Patient-Derived Subcutaneous Xenograft and Organotypic Slice Cultures in Hormone-Naive Primary Prostate Cancer Preclinical Modeling: A Single-Institution Experience. *Life (Basel)* **15**, 1719 (2025).
28. *Davidian, M., & Giltinan, DAVID .M (1995). Nonlinear Models for Repeated Measurement Data (1st Ed.). Routledge. Https://Doi.Org/10.1201/9780203745502*.
29. Li, S. *et al.* The suppression of ox-LDL-induced inflammatory cytokine release and apoptosis of HCAECs by long non-coding RNA-MALAT1 via regulating microRNA-155/SOCS1 pathway. *Nutr Metab Cardiovasc Dis* **28**, 1175–1187 (2018).
30. Hu, H. *et al.* Elevated COX-2 Expression Promotes Angiogenesis Through EGFR/p38-MAPK/Sp1-Dependent Signalling in Pancreatic Cancer. *Sci Rep* **7**, 470 (2017).

31. Wilson, S., Qi, J. & Filipp, F. V. Refinement of the androgen response element based on ChIP-Seq in androgen-insensitive and androgen-responsive prostate cancer cell lines. *Sci Rep* **6**, 32611 (2016).
32. Li, M.-H., Jang, J.-H. & Surh, Y.-J. Nitric oxide induces apoptosis via AP-1-driven upregulation of COX-2 in rat pheochromocytoma cells. *Free Radic Biol Med* **39**, 890–899 (2005).
33. Sun, Y., Chen, J. & Rigas, B. Chemopreventive agents induce oxidative stress in cancer cells leading to COX-2 overexpression and COX-2-independent cell death. *Carcinogenesis* **30**, 93–100 (2009).
34. Notoya, K. *et al.* The induction of cell death in human osteoarthritis chondrocytes by nitric oxide is related to the production of prostaglandin E2 via the induction of cyclooxygenase-2. *J Immunol* **165**, 3402–3410 (2000).
35. Sobolewski, C., Cerella, C., Dicato, M., Ghibelli, L. & Diederich, M. The role of cyclooxygenase-2 in cell proliferation and cell death in human malignancies. *Int J Cell Biol* **2010**, 215158 (2010).
36. Li, X. *et al.* Role of COX-2/PGE2 signaling pathway in the apoptosis of rat ovarian granulosa cells induced by MEHP. *Ecotoxicol Environ Saf* **254**, 114717 (2023).
37. Bocca, C., Bozzo, F., Bassignana, A. & Miglietta, A. Antiproliferative effect of a novel nitro-oxy derivative of celecoxib in human colon cancer cells: role of COX-2 and nitric oxide. *Anticancer Res* **30**, 2659–2666 (2010).
38. Bell, C. R. *et al.* Chemotherapy-induced COX-2 upregulation by cancer cells defines their inflammatory properties and limits the efficacy of chemoimmunotherapy combinations. *Nat Commun* **13**, 2063 (2022).

39. Kurtova, A. V. *et al.* Blocking PGE2-induced tumour repopulation abrogates bladder cancer chemoresistance. *Nature* **517**, 209–213 (2015).
40. Zelenay, S. *et al.* Cyclooxygenase-Dependent Tumor Growth through Evasion of Immunity. *Cell* **162**, 1257–1270 (2015).
41. Khan, A. F. *et al.* Androgen Receptor in Hormone Receptor-Positive Breast Cancer. *Int J Mol Sci* **25**, 476 (2023).
42. Wei, L. *et al.* Pharmacological Targeting of Androgen Receptor Elicits Context-Specific Effects in Estrogen Receptor-Positive Breast Cancer. *Cancer Res* **83**, 456–470 (2023).
43. Huang, Y. *et al.* Downregulation of malic enzyme 3 facilitates progression of gastric carcinoma via regulating intracellular oxidative stress and hypoxia-inducible factor-1α stabilization. *Cell Mol Life Sci* **81**, 375 (2024).
44. Nowak, J. A. *et al.* Improved Survival With Adjuvant Cyclooxygenase 2 Inhibition in PIK3CA-Activated Stage III Colon Cancer: CALGB/SWOG 80702 (Alliance). *J Clin Oncol* **42**, 2853–2859 (2024).
45. Zhang, G. Q. *et al.* Predictive Role of Circulating Tumor DNA in Stage III Colon Cancer Treated With Celecoxib: A Post Hoc Analysis of the CALGB (Alliance)/SWOG 80702 Phase 3 Randomized Clinical Trial. *JAMA Oncol* **12**, 149–158 (2026).

## Supplementary Files

This is a list of supplementary files associated with this preprint. Click to download.

- DeMartinoetalSupplementaryMaterials25.09.2026.pdf